Macromolecular Chemistry and Physics
www.mcp-journal.de

Varying the Hydrogen Bonding Strength in Phenolic/PEO-*b*-PLA Blends Provides Mesoporous Carbons Having Large Accessible Pores Suitable for Energy Storage

*Jheng-Guang Li, Po-Yuan Lee, Mahmoud M. M. Ahmed, Mohamed Gamal Mohamed, and Shiao-Wei Kuo**

In this study, mesoporous carbons are prepared by using a resol-type phenolic resin as the carbon source and poly(ethylene oxide-*b*-lactic acid) (PEO-*b*-PLA) copolymer as the template, with a process of thermal curing, calcination, carbonization, and activation. The structures of these mesoporous carbons are strongly influenced by the self-assembled structures formed from phenolic/PEO-*b*-PLA blends, varying from double-gyroid, to cylinder, and finally to spherical micelle structures upon increasing the phenolic concentrations. The large pores (>20 nm) and high surface areas (>1000 $m^2 g^{-1}$) of these activated mesoporous carbons arise because the phenolic resin interacts only with the PEO segment (i.e., not with the PLA segment) through hydrogen bonding; thus, the relative wall thickness of the phenolic matrix decreases after template removal (thereby increasing the pore size), similar to the behavior of the poly(ethylene oxide-*b*-styrene) template system. Furthermore, these mesoporous carbons display efficient energy storage capacities of up to 200 F g^{-1} at 5 mV s^{-1}, with excellent stabilities after 5000 charge/discharge cycles at 20 A g^{-1}. Thus, this facile approach provides large and well-ordered mesoporous carbons suitable for energy storage applications.

1. Introduction

Mesoporous materials are becoming attractive materials for their various applications in, e.g., drug delivery, energy storage, and energy generation, as well as other fields.[1–8] In energy storage devices, mesoporous carbons can function as efficient electron transfer media to improve the performance of electric double-layer capacitors (EDLCs).[9] Furthermore, the blending of a self-assembled block copolymer with the carbon source (e.g., phenolic resin) is becoming more widespread. This method has the advantage of providing well-ordered mesoporous structures that can be used efficiently in various applications.[10,11]

Typically, a block copolymer that forms a self-assembled structure is mixed with a carbon source to obtain various dimensional carbon structures. The blending of a commercial Pluronic-type triblock copolymer, such as poly(ethylene oxide-*b*-propylene oxide-*b*-ethylene oxide), as the template is the method used most widely to prepare mesoporous materials.[12–19] Because of limitations in molecular weight and composition, it can, however, be difficult to prepare mesoporous materials having pore sizes of greater than 10 nm when using Pluronic-type triblock copolymers. Block copolymers featuring long hydrophobic segments and high molecular weight—for instance, poly(ethylene oxide-*b*-styrene) (PEO-*b*-PS)[20,21] and poly(ethylene oxide-*b*-methyl methacrylate) (PEO-*b*-PMMA)[22]—are promising candidates as templates to prepare large-pore-size mesoporous carbons. For example, Zhao et al. prepared mesoporous carbons with long-range order, large surface areas (>1500 $m^2 g^{-1}$), and large pores (≈23 nm) when using PEO_{125}-*b*-PS_{230} as the template as displayed in Scheme S1a–c in the Supporting Information.[21] With PEO_{125}-*b*-$PMMA_{114}$ as the template, they obtained mesoporous carbons having large surface areas (>1500 $m^2 g^{-1}$) and pores (≈10 nm)[22] when applying resol as the carbon source. Mesoporous carbons with smaller pores but thicker walls were obtained when using PEO-*b*-PMMA as the template, rather than PEO-*b*-PS, because the phenolic OH units could interact strongly with the PEO segment (interassociation equilibrium constant (K_A) = 286)[23] and weakly with the PMMA C=O units (K_A = 20)[24,25] through hydrogen bonding, but not with the hydrophobic PS segment. Indeed, the PS block segment would undergo complete microphase

Dr. J.-G. Li, P.-Y. Lee, Dr. M. M. M. Ahmed, Dr. M. G. Mohamed, Prof. S.-W. Kuo
Department of Materials and Optoelectronic Science
Center of Crystal Research, National Sun Yat-Sen University
Kaohsiung 80424, Taiwan
E-mail: kuosw@faculty.nsysu.edu.tw
Prof. S.-W. Kuo
Department of Medicinal and Applied Chemistry
Kaohsiung Medical University
Kaohsiung 807, Taiwan
The ORCID identification number(s) for the author(s) of this article can be found under https://doi.org/10.1002/macp.202000040.

DOI: 10.1002/macp.202000040

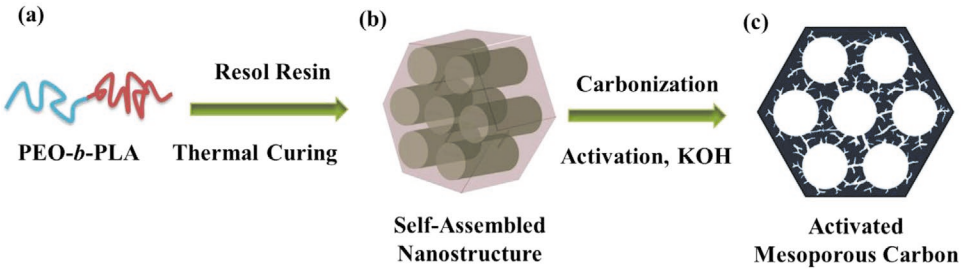

Scheme 1. Fabrication of c) mesoporous carbons and activated mesoporous carbons (with KOH) through templation using a) a PEO-*b*-PLA copolymer and b) reaction-induced microphase separation mechanism and phenolic/PEO-*b*-PLA blends.

separation from the miscible phenolic/PEO domains and, thereby, induce larger pores and thinner walls from the phenolic matrix after the removal of the template. Modification of the chain end of the PEO block segment (e.g., as PEO-Br) is necessary for use as an atom transfer radical polymerization macroinitiator for the syntheses of both PEO-*b*-PS and PEO-*b*-PMMA templates.[20–22] In previous studies, we systematically studied the preparation of mesoporous carbons from both novolac- and resol-type phenolic as carbon sources when using poly(ethylene oxide-*b*-caprolactone) (PEO-*b*-PCL) as templates as displayed in Scheme S1d–f in the Supporting Information.[26–32] These PEO-*b*-PCL copolymers were readily synthesized through ring opening polymerization (ROP) of caprolactone as the monomer when using commercial PEO-OH homopolymers as macroinitiators without the need for modification of the chain end.[26–32] Nevertheless, the largest pores of the resulting mesoporous carbons were only ≈12 nm when using PEO-*b*-PCL as templates, because OH units of phenolic also interacted strongly with PCL C=O units (K_A = 116), similar to the behavior as using PEO-*b*-PMMA template; thus, the wall thickness of the phenolic matrix increased as a result of forming phenolic/PCL domains, thereby decreasing the pore size.[31,32]

From a consideration of potential monomers for ROP that would provide weakly hydrogen bonding acceptor units, L-lactide (LLA) appeared to be a promising candidate for use in the template because the K_A value for phenolic/PLLA blend is <10.[33] Nevertheless, the crystallization behavior of PEO-*b*-PLLA copolymers used as the template would strongly affect the resulting self-assembled mesostructures because the free energy of crystallization is generally lower than microphase separation process; accordingly, lamellar structures have generally been observed from the PLLA crystallization.[34] Fortunately, crystalline PLLA segments can readily be changed into amorphous PLA segments when incorporating an equal number of D- and L-forms in which the overall PLA segment is not chiral.[35] In this study, we synthesized a PEO_{114}-*b*-PLA_{94} diblock copolymer through simple ROP when using commercial PEO-OH as a macroinitiator. We then prepared mesoporous carbons by using resol as the carbon source and the PEO-*b*-PLA as a template, through a process of thermal curing, calcination, carbonization, and activation (**Scheme 1**). These facile methods for preparing the templating PEO-*b*-PLA copolymer and for synthesizing large-pore (>20 nm) mesoporous carbons appear to be very applicable for energy storage and generation.

2. Results and Discussion

2.1. Characterization of Phenolic/PEO-*b*-PLA Blends

We synthesized the amphiphilic PEO_{114}-*b*-PLA_{94} diblock copolymer for use as a template and calculated its molecular weight using ^{1}H NMR spectroscopy (Figure S1, Supporting Information). Signals appeared at 3.65 ppm corresponding to the PEO methylene (CH_2) protons and at 5.14 and 1.58 ppm for the methine (CH) and methyl (CH_3) protons, respectively, for PLA segment, with the ratio of the integrated areas of the peaks for the methine and methyl protons being 1:3. The molecular weight of PEO_{114}-*b*-PLA_{94} was determined from the area ratio of the signals from the CH or CH_3 units for PLA segment and the CH_2 units of the PEO segment. Activated mesoporous carbons were prepared by dissolving phenolic/PEO-*b*-PLA blends in THF transforming the mesophase gradually into highly ordered structures through EISA, thermal curing, carbonization, and activation, as displayed in Scheme 1.

Fourier-transform infrared (FTIR) spectroscopy was used to investigate the hydrogen bonding interactions in phenolic/PEO-*b*-PLA blends (**Figure 1**). The FTIR spectrum of the pure resol-type phenolic resin displayed (Figure 1a) two major signals: one for free OH unit at 3525 cm^{-1} and the other at 3350 cm^{-1} because of self-association OH···OH hydrogen bonding. The intensity for free OH units gradually decreased and that for the self-association hydrogen bonding shifted to lower wavenumber (≈3200 cm^{-1}) upon increasing PEO-*b*-PLA concentration, implying that the weak self-association OH···OH hydrogen bonds transformed to strong inter-association hydrogen bonding of the OH with the C–O–C units.[36] We did not observe evidence for inter-molecular hydrogen bonding of phenolic OH units with the C=O units of the PLA segment. In Figure 1b, the pure PLA segment provided a signal for its free C=O units at 1756 cm^{-1}; no peak shifting occurred or any new shoulder peak appeared upon increasing the phenolic concentration in the phenolic/PEO-*b*-PLA blends. This result is quite different from those found for other polymers containing C=O groups when blended with phenolic resin, including PCL (K_A = 116),[16] polyvinyl acetate (K_A = 83),[36] para-aminosalicylic acid (K_A = 64),[37] and PMMA (K_A = 20),[24] and their homopolymers. The strong intramolecular C–H···O=C hydrogen bonding in the PLA segment resulted in the lower hydrogen bonded acceptor ability (K_A < 10).[33] Furthermore, a band near 1100 cm^{-1} characterized the intermolecular hydrogen bonding in the phenolic/PEO

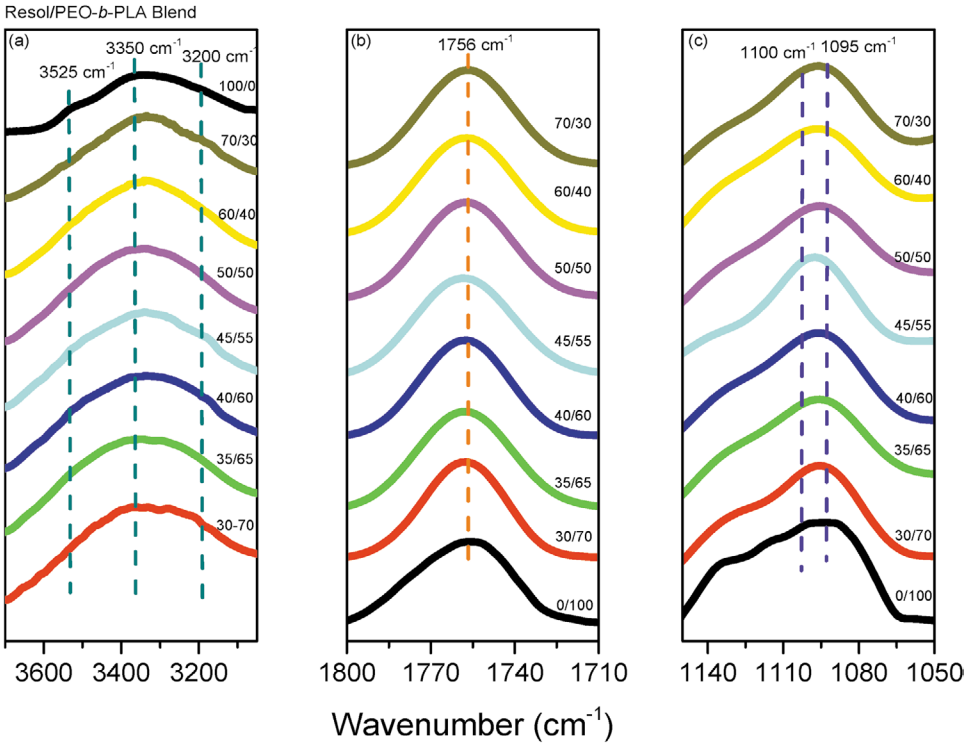

Figure 1. FTIR spectra, recorded at room temperature, of various phenolic/PEO-*b*-PLA blends: a) OH stretching, b) C=O, and c) C—O—C regions.

domains. Figure 1c presents the FTIR spectral range containing the signal for the ether absorptions of the phenolic/PEO-*b*-PLA blends. Pure PEO-*b*-PLA provided a characteristic band at 1100 cm^{-1} corresponding to the C—O—C absorption of its PEO segment. Upon increasing the phenolic concentration, this band shifted gradually to 1095 cm^{-1}.[32] As a result, we suspect that the phenolic OH units interacted only with the PEO segment, and not with the PLA segment, similar to the behavior of phenolic/PEO-*b*-PS blend systems.[20,21]

Figure 2a,d,g presents the small-angle X-ray scattering (SAXS) profiles of various phenolic/PEO-*b*-PLA blends measured at room temperature (red lines). The scattering pattern of the phenolic/PEO-*b*-PLA = 40/60 blend (Figure 2a) featured a peak ratio of $\sqrt{6}$:$\sqrt{8}$:$\sqrt{20}$:$\sqrt{22}$, indicative of a bicontinuous gyroid structure, with the first scattering peak locating at a value of $\sqrt{6}q^*$ of 0.203 nm^{-1} (d = 30.93 nm). Increasing the phenolic concentration to give the phenolic/PEO-*b*-PLA = 50/50 blend caused the scattering pattern (Figure 2d) to have a peak ratio of 1:$\sqrt{3}$:$\sqrt{4}$:$\sqrt{7}$, representing the high order of the hexagonally packed cylinder structure, the first peak at a value of q^* of 0.201 nm^{-1} (d = 31.24 nm). For the phenolic/PEO-*b*-PLA = 60/40 blend, the scattering pattern (Figure 2g) featured only weak and broad peaks at a ratio of 1:$\sqrt{3}$, implying the presence of a short-range-ordered wormlike or spherical micelle structure, with the first peak at a value of q^* of 0.194 nm^{-1} (d = 32.37 nm). Thus, an order–order morphological transition occurred from a gyroid, to a cylinder, and finally to a spherical micelle structure, with the domain size (d-spacing) increasing, upon increasing the phenolic concentration, characteristic of wet-brush behavior in the phenolic/PEO-*b*-PLA blends, as has been observed also for phenolic/PEO-*b*-PCL blend systems.[26–32]

2.2. Characterization of Mesoporous Carbons Templated by PEO-*b*-PLA Copolymer

We thermally cured the phenolic matrix at 150 °C for 24 h and then performed the thermal calcination at 700 °C to remove PEO-*b*-PLA template and produce the mesoporous carbons. Figure 2a,d,g also presents the SAXS profiles of the mesoporous carbons obtained from the corresponding phenolic/PEO-*b*-PLA blends, measured at room temperature (green lines). After removal of the PEO-*b*-PLA template, all of the signals became sharper (the result of greater electron density contrast upon pore formation), but the peak ratios did not change, implying that the original self-assembled structures and shapes were maintained. In addition, the first peaks were shifted to higher values of q after thermal calcination, because of the removal of hydrogen, oxygen, and carbon atoms from the mesoporous matrix, revealing that the d-spacing shrunk during thermal pyrolysis. For example, the SAXS pattern of the mesoporous carbon obtained from the phenolic/PEO-*b*-PLA = 40/60 blend exhibited peaks (Figure 2a, green line) in the characteristic $\sqrt{6}$:$\sqrt{8}$:$\sqrt{20}$:$\sqrt{22}$ ratio, indicating that the gyroid structure was maintained after thermal calcination, as confirmed from the transmission electron microscopy (TEM) images viewed from the [111] and [211] planes (Figure 2b,c, respectively). The first peak corresponding to $\sqrt{6}q^*$ from [211] had shifted to 0.33 nm^{-1} (d = 19.03 nm); the cell parameter a was 46.61 nm, calculated using the equation $a = 6^{1/2}d_{211}$. The SAXS pattern of the mesoporous carbon obtained from phenolic/PEO-*b*-PLA = 50/50 blend retained the peaks at a 1:$\sqrt{3}$:$\sqrt{4}$:$\sqrt{7}$ ratio (Figure 2d, green line), corresponding to a hexagonally packed cylinder structure, consistent with the TEM images in

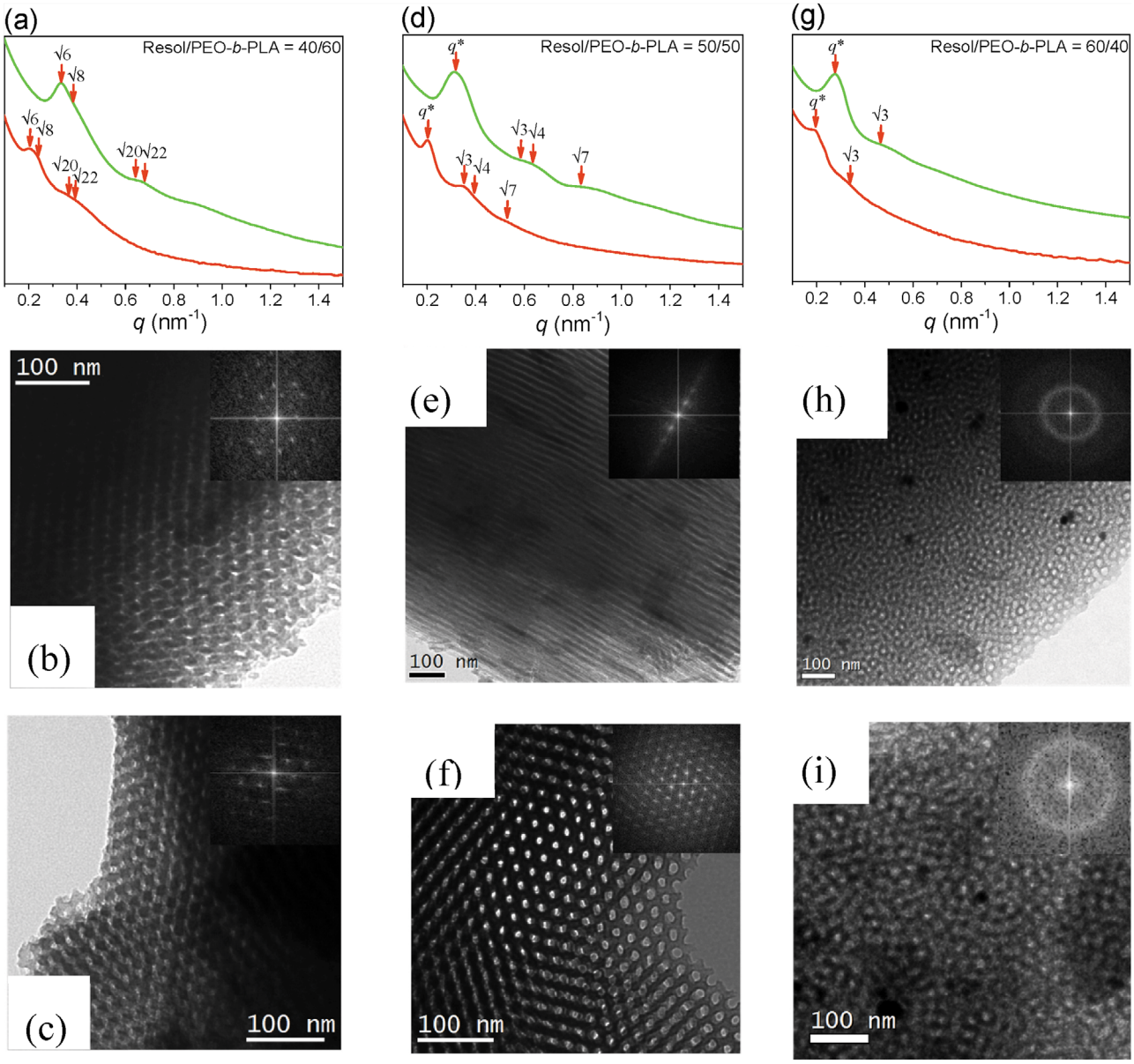

Figure 2. SAXS and TEM analyses of phenolic/PEO-*b*-PLA blends, and corresponding mesoporous carbons, obtained at ratios of a–c) 40/60, d–f) 50/50, and g–i) 60/40.

Figure 2e (side view) and Figure 2f (top view); the first peak had shifted to 0.31 nm^{-1} (d = 20.25 nm) after thermal calcination. Finally, the SAXS pattern of the mesoporous carbon obtained from the phenolic/PEO-*b*-PLA = 60/40 blend featured peaks at a 1:√3 ratio (Figure 2g, green line), suggesting a short-range-ordered wormlike or spherical micelle structure, consistent with the TEM images in Figure 2h,i; the first peak had shifted to 0.27 nm^{-1} (d = 23.25 nm) after thermal calcination.

Figure 3 displays N_2 sorption isotherms of these three mesoporous carbons. The typical type-IV curves observed for the mesoporous carbons obtained from both the phenolic/PEO-*b*-PLA = 40/60 and 50/50 blends underwent sharp capillary condensations at relative pressures in the range from 0.8 to 1.0, thereby revealing H_1-like hysteresis loops, suggesting common mesoporous structures with large and cylindrical pores. The H_2-like hysteresis loops for the mesoporous carbon obtained from the phenolic/PEO-*b*-PLA = 60/40 blend, suggested a common cage-like mesoporous structure, as displayed in Figure 3a. These findings are consistent with the SAXS and TEM data. The mean pore size distributions of the mesoporous carbons obtained from the phenolic/PEO-*b*-PLA = 40/60, 50/50, and 60/40 blends, based on the Harkins and Jura model, were 20.7, 18.5, and 21.0 nm, respectively, based on Figure 3b. Thus, the pore sizes (>21 nm) of the mesoporous carbons templated by PEO_{114}-*b*-PLA_{94} (M_n = 10 600 g mol^{-1}) were similar to those (≈23 nm) obtained when using PEO_{125}-*b*-PS_{230} (M_n = 29 000 g mol^{-1}) as the template, albeit of much higher molecular weight.[21] The SAXS patterns and N_2 sorption isotherms

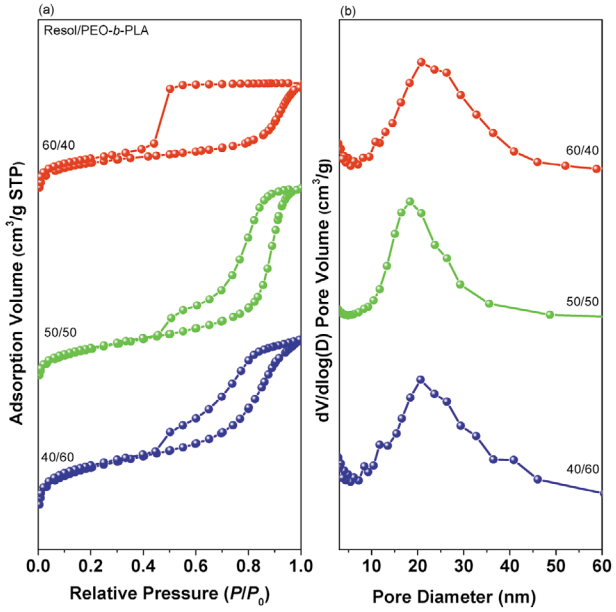

Figure 3. a) N_2 adsorption/desorption hysteresis isotherms and b) pore size distributions of mesoporous carbons obtained from various phenolic/PEO-*b*-PLA blends.

of the mesoporous carbons obtained from the phenolic/PEO-*b*-PLA = 30/70 and 70/30 blends (Figure S3, Supporting Information) reveal short-range-ordered mesoporous structures; thus, our focus in this study was aimed primarily at the mesoporous carbons obtained from the phenolic/PEO-*b*-PLA = 40/60, 50/50, and 60/40 blends. **Table 1** summarizes the pore sizes, surface areas, and pore volumes of the mesoporous carbons.

2.3. Characterization of Activated Mesoporous Carbon

Because an EDLC supercapacitor stores its electrical energy through a static electricity effect, we first performed an activation process with these mesoporous carbons to increase their mesoporous surface areas for electrolyte adsorption. **Figure 4**a,c,e displays the SAXS patterns of the mesoporous carbons (green lines) and activated mesoporous carbons (blue lines) obtained from the various phenolic/PEO-*b*-PLA blends. The patterns of all of these activated mesoporous carbons retained their peak ratios after performing the KOH activation process, suggesting that their porous structures remained. For example, the activated mesoporous carbon derived from phenolic/PEO-*b*-PLA = 40/60 (Figure 4a, blue line) retained the signals at a $\sqrt{6}$:$\sqrt{8}$:$\sqrt{20}$:$\sqrt{22}$ ratio of a typical double-gyroid structure, as confirmed in the TEM image observed from the [111] plane (Figure 4b). The hexagonal cylinder structure, revealed by signals at a 1:$\sqrt{3}$:$\sqrt{4}$:$\sqrt{7}$ ratio (Figure 4c, blue line), for the activated mesoporous carbon derived from phenolic/PEO-*b*-PLA = 50/50, was also confirmed by its top-view TEM image (Figure 4d). The mesoporous carbon featuring the spherical micelles retained its mesophase after the activation process, with a peak ratio of 1:$\sqrt{3}$ (Figure 4e, blue line), as confirmed in the TEM image in Figure 4f. Thus, the SAXS and TEM analyses indicated that all of the mesoporous structures were maintained; they had extremely stable structures, even under the strongly basic conditions and high temperature employed during their activation.

Figure 5 displays the N_2 adsorption/desorption isotherms recorded after the activation process to measure the Brunauer–Emmett–Teller (BET) surface areas and pore sizes. Interestingly, the adsorption/desorption isotherms of the mesoporous carbons were retained after their activation: type IV with H_1 hysteresis loops for the structures derived from phenolic/PEO-*b*-PLA = 40/60 and 50/50 (Figure 5a,c) and a H_2 hysteresis loop for the structure derived from phenolic/PEO-*b*-PLA = 60/40 (Figure 5e). Furthermore, the pore sizes of mesoporous carbons were similar before and after activation: decreasing from 20.7 to 17.6 nm for the gyroid structure (Figure 5b), remaining the same for the cylinder structure (both 18.5 nm, Figure 5d), and decreasing from 21.0 to 20.6 nm for the spherical micelle structure (Figure 5f). Table 1 also lists the textural properties of these three activated mesoporous carbons; their surface areas all increased significantly after activation. Thus, the activation treatment not only decreased the pore sizes but also created new micropores that enhanced the surface areas, and these surface areas and pore sizes were larger than those of other previously reported activated mesoporous carbons.[32] For example, an activated mesoporous carbon obtained from the same resol-type of phenolic resin as the carbon source, but templated by

Table 1. Textural properties of mesoporous carbons and activated mesoporous carbons prepared from various resol/PEO-*b*-PLA blends.

Mesoporous carbon	d[a)] [nm]	Pore size[b)] [nm]	S_{BET}[b)] [$m^2\ g^{-1}$]	S_M[b)] [$m^2\ g^{-1}$]	V_{total} [$cm^3\ g^{-1}$]	V_M [$cm^3\ g^{-1}$]	Structure
30/70	–	–	470	88	0.289	0.073	Disorder
40/60	19.03	20.7	532	113	0.286	0.121	Gyroid
50/50	20.25	18.5	584	174	0.627	0.416	Cylinder
60/40	23.25	21.0	487	116	0.378	0.186	Sphere
70/30	25.12	–	483	88	0.318	0.196	Disorder
Activated mesoporous carbon							
40/60		17.6	1055	915	0.629	0.455	Gyroid
50/50		18.5	1182	921	0.849	0.459	Cylinder
60/40		20.6	1042	864	0.664	0.429	Sphere

[a)]SAXS pattern by $d = 2\pi/q^*$ equation; [b)]S_{BET} is the total BET surface area and S_M is the micropore surface area.

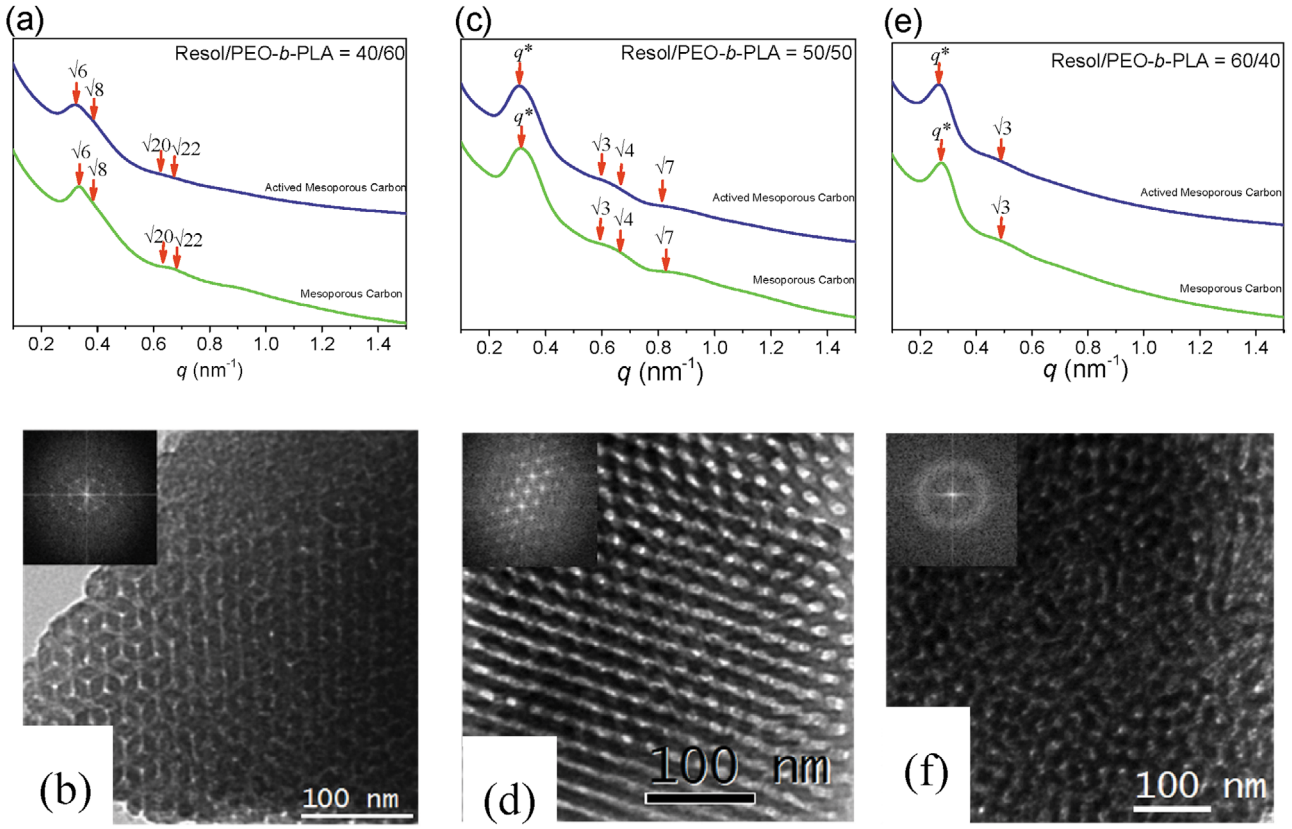

Figure 4. SAXS patterns and TEM images of mesoporous carbons and corresponding activated mesoporous carbons obtained from phenolic/PEO-*b*-PLA blends of a,b) 40/60, c,d) 50/50, and e,f) 60/40.

a PEO-*b*-PCL copolymer, featured pore sizes of only 15.6 nm for the cylinder structure and 14.1 nm for the gyroid structure, even though the molecular weight for PEO-*b*-PCL copolymer (M_n = 15 000 g mol^{-1})[32] was higher than that of the PEO-*b*-PLA copolymer (M_n = 10 600 g mol^{-1}) used in this study. This result can be understood by considering that the OH units of the phenolic not only interacted with the C—O—C units in the PEO segment but also with the C=O units in the PCL segment; thus, the wall thickness of the phenolic matrix increased and the pore size decreased after thermal calcination. In contrast to the PEO-*b*-PCL template, for the PEO-*b*-PLA copolymer the phenolic resin could interact only with the PEO segment, and not with the C=O units in the PLA segment; thus, in this present study, the relative wall thickness of the phenolic matrix decreased, corresponding to an increase in the pore size.

Because these activated mesoporous carbons had high surface areas, we suspected they would be highly useful in various energy-related applications.[38] We investigated these activated mesoporous carbons for their ability to boost the efficiencies of electrochemical energy storage.[39,40] We measured their performance in a three-electrode cell using 6.0 M KOH as a basic electrolyte; these conditions provided a green medium having a wide potential range for cyclic voltammetry (CV), from –0.9 to –0.1 V, for all the activated mesoporous carbons (**Figure 6**).[41] All of the activated mesoporous carbons derived from the various PEO- *b*-PLA ratios provided similar EDLC curves within the investigated range, suggesting uniform carbon structures after activation at all of the ratios.[42,43] Furthermore, we observed evidence for a mild pseudocapacitor reaction at the edges of the curves, possibly due to functionalization with oxygen and nitrogen atoms during the high-temperature activation process.[44,45] These results are typical and similar to those we found previously for structures formed when using a PEO-*b*-PCL copolymer as the template.[42] In addition, the capacitances of the electrode materials obtained at all activated carbon ratios were quite similar (Figure S4, Supporting Information), suggesting that the different mesoporous carbons did not possess different chemical structures and they did not display different electrochemical behavior. This also was supported by the similar EDLC as well as PC performance obtained at all investigated scan rates. The achieved capacitances for the gyroid, cylinder, and spherical activated mesoporous carbons reached 190, 200, and 185 F g^{-1}, respectively, at 5 mV s^{-1}. These values are higher than those of related 2D materials, including exfoliated graphite materials heated at 2000 °C[46] and exfoliated MoS_2.[47] They are also higher than those of the mesoporous carbons templated by a PEO-*b*-PCL copolymer under the same conditions,[32] ten times higher than those of a mesoporous poly(cyanate ester) silsesquioxane,[48] and higher than those of nutshell carbon and lignin-derived carbons (which displayed capacitances of 45 F g^{-1} @ 1 mV s^{-1} and 100 F g^{-1} @ 5 mV s^{-1}, respectively).[49] We suspect that the high performance of these mesoporous carbons templated by the PEO-*b*-PLA copolymer arose mainly from their well-designed structures, which

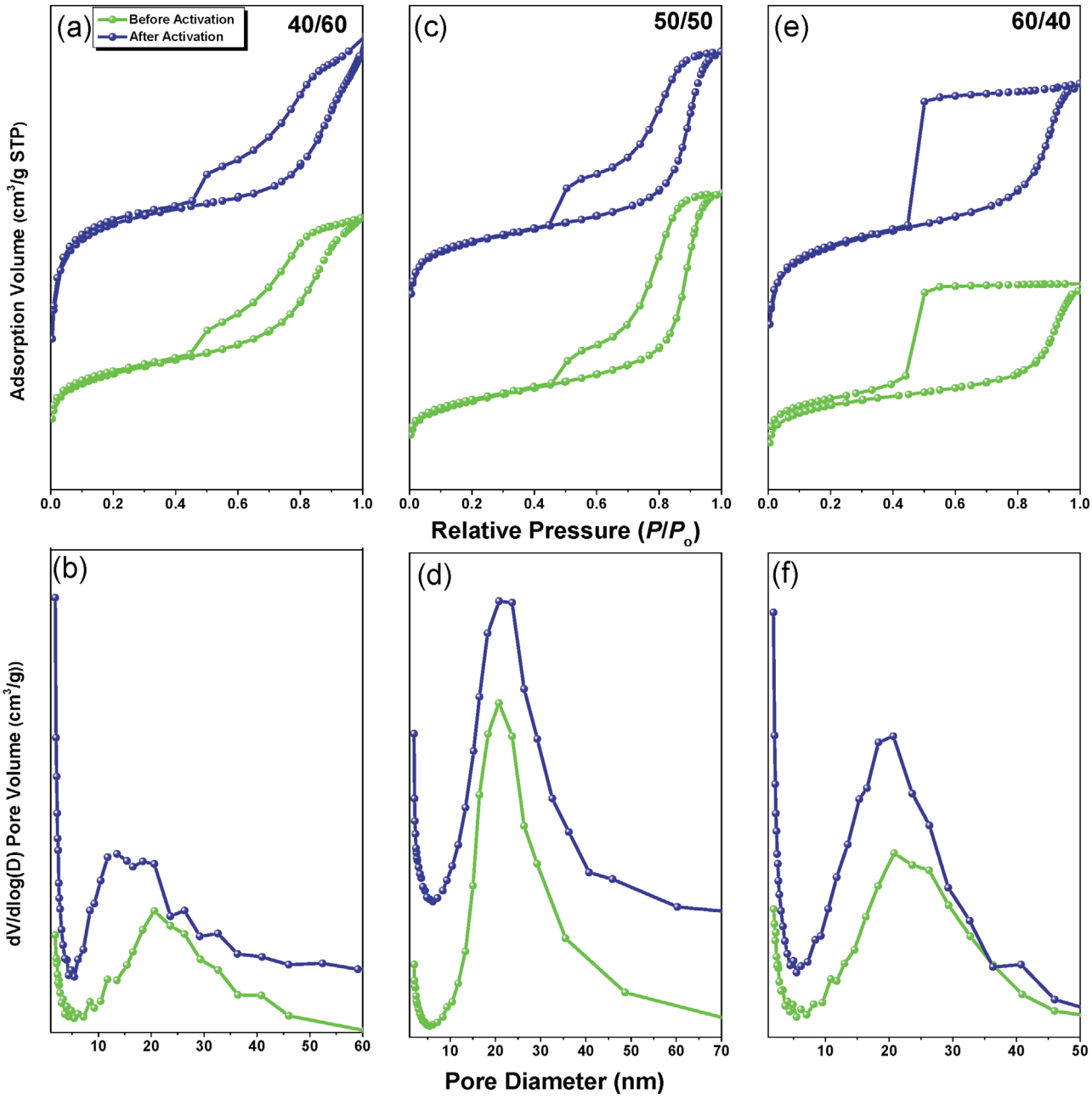

Figure 5. a,c,e) N_2 adsorption/desorption hysteresis isotherms and b,d,f) the pore size distributions of mesoporous carbons and corresponding activated mesoporous carbons obtained from various phenolic/PEO-*b*-PLA blends of a,b) 40/60, c,d) 50/50, and e,f) 60/40.

resulted from the self-assembly of the block copolymer and were retained during their activation processing. Moreover, the charge/discharge curves revealed symmetric behavior, without any internal resistance drop, for the mesoporous structures formed at the various ratios and recorded under various current densities (Figure 6b,c). Thus, the activated uniform structures provided regular and nonresistive electron pathways. In addition, Figure 6d displays the Coulombic efficiencies with excellent stabilities at 20 A g^{-1} after 5000 cycles within the investigated potential range; for the gyroid, cylinder, and spherical micelle activated mesoporous carbons, the Coulombic efficiencies were 92%, 95%, and 89%, respectively. These excellent stabilities are superior to those of other activated frameworks, which have yielded stabilities of only 84%.[50,51]

3. Conclusions

We have prepared various types of mesoporous carbons templated by a PEO-*b*-PLA copolymer, which we synthesized through simple ROP, and a resol-type phenolic resin as the carbon source. Changes in the types of competing hydrogen

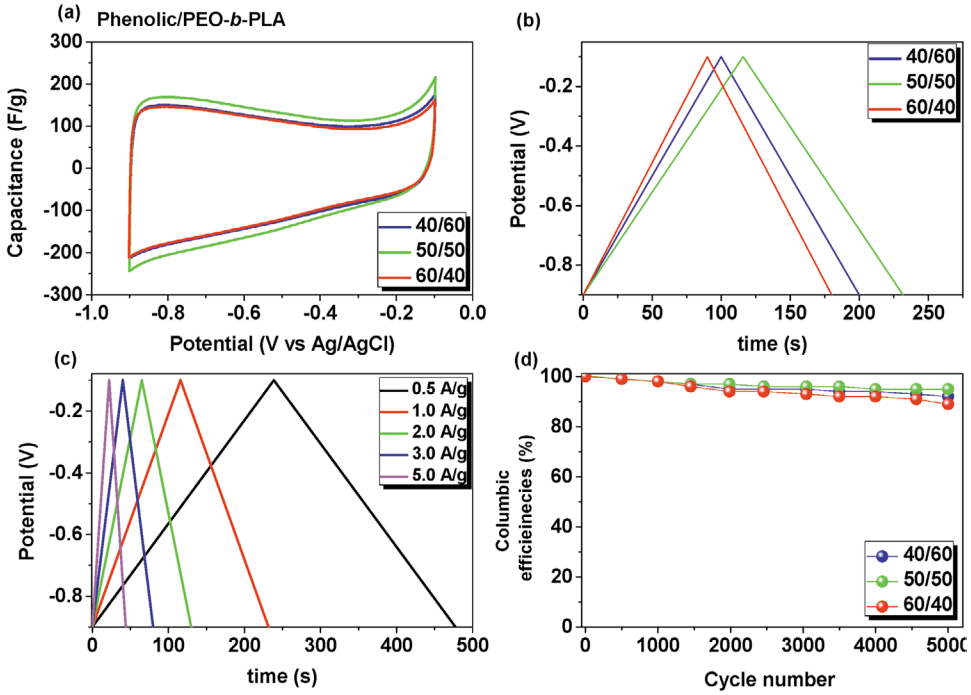

Figure 6. a) CV traces of activated mesoporous carbons having gyroid, cylinder, and spherical micelle structures, measured at 5 mV s^{-1}. b,c) Charge/discharge curves recorded for b) the three samples measured at 1 A g^{-1} and c) the cylinder-structured activated mesoporous carbon measured at various current densities. d) Coulombic efficiencies of the three activated mesoporous carbons, measured at 20 A g^{-1} for 5000 cycles.

bonding interactions of the phenolic/PEO and phenolic/PLA domains resulted in the self-assembled structures of mesoporous carbons ranging from double-gyroid, to cylinder, and finally to spherical micelle structures upon increasing the concentration of the phenolic. After activation, the activated mesoporous carbons possessed large pores (>20 nm) and high surface areas (>1000 m^2 g^{-1}); they also displayed highly efficient capacitance behavior, with excellent stability of up to 95% after 5000 cycles. This facile method for preparing stable mesoporous carbon structures, through adjustments in the strength of hydrogen bonding interactions, leads to materials displaying efficient electrochemical performance.

4. Experimental Section

Materials: The PEO_{114}-*b*-PLA_{94} amphiphilic diblock copolymer was prepared through ROP of D,L-lactic acid as the monomer, monomethoxy-poly(ethylene oxide) (PEO_{114}) as the macroinitiator, and stannous(II) octoate as the catalyst. Briefly, the D,L-lactic acid monomer (5.00 g, 55.55 mmol) was degassed, mixed with PEO (2.12 g, 0.424 mmol) in the presence of 100 mL of dry toluene and a few drops of the catalyst, and stirred continuously under a N_2 atmosphere at 130 °C for 24 h. The resulting PEO_{114}-*b*-PLA_{94} copolymer was dissolved in dry dichloromethane and precipitated three times in an excess solvent of cold n-hexane to remove unreacted monomers. Finally, the white solid was collected and dried under vacuum at 40 °C for 12 h. The chemical structure and molecular weight of PEO_{114}-*b*-PLA_{94} diblock copolymer were determined by ^{1}H NMR and gel permeation chromatography measurements (Figures S1 and S2, Supporting Information). The resol-type of phenolic resin (molecular weight: ≈500 g mol^{-1}) was synthesized through condensation of phenol with formaldehyde in NaOH medium.[26–32]

Mesoporous Carbon and Activated Mesoporous Carbon: Various amounts of resol phenolic/PEO-*b*-PLA blends were dissolved in tetrahydrofuran (THF) and stirred for 24 h at room temperature. The mixtures were poured into dishes and then the THF was evaporated over 8 h at room temperature to enable evaporation-induced self-assembly (EISA). The dish was transferred to vacuum oven for thermal curing of resol phenolic resin at 150 °C for 24 h. The mesoporous carbon was obtained after template removal by thermal calcination for 3 h under N_2 (at 1 °C min^{-1}, up to 700 °C). The mesoporous carbon was dispersed in $KOH_{(aq)}$ at 60 °C for 3 h, dried at 100 °C for 12 h, and then re-heated under N_2 at 700 °C (Scheme 1). The resulting activated mesoporous carbons were washed to neutral pH and dried under vacuum.

Supporting Information

Supporting Information is available from the Wiley Online Library or from the author.

Acknowledgements

This study was supported financially by the Ministry of Science and Technology, Taiwan, under contracts MOST 108-2221-E-110-014-MY3, 106-2221-E-110-067-MY3, and 108-2638-E-002-003-MY2.

Conflict of Interest

The authors declare no conflict of interest.

Keywords

diblock copolymers, mesoporous carbon, self-assembly, supercapacitors

Received: January 31, 2020
Revised: March 18, 2020
Published online: April 8, 2020

[1] J. Liu, L. Xie, J. Deng, Y. Gong, G. Tang, H. Bai, Y. Wang, *Chem. Mater.* **2019**, *31*, 7186.
[2] K. Nomura, H. Nishihara, N. Kobayashi, T. Asada, T. Kyotani, *Energy Environ. Sci.* **2019**, *12*, 1542.
[3] A. Pockett, D. Raptis, S. M. P. Meroni, J. A. Baker, T. M. Watson, M. Carnie, *J. Phys. Chem. C* **2019**, *123*, 11414.
[4] Q. Y. Guo, B. X. Zhang, X. Feng, X. Y. Yan, Z. Su, S. Z. D. Cheng, K. Yue, *Macromol. Rapid Commun.* **2020**, *41*, 1900534.
[5] Y. Yamauchi, T. Nagaura, A. Ishikawa, T. Chikyow, S. Inoue, *J. Am. Chem. Soc.* **2008**, *130*, 10165.
[6] M. Nandi, J. Mondal, K. Sarker, Y. Yamauchi, A. Bhaumik, *Chem. Commun.* **2011**, *47*, 6677.
[7] B. Jiang, Y. Guo, J. Kim, A. E. Whitten, K. Wood, K. Kani, A. E. Rowan, J. Henzie, Y. Yamauchi, *J. Am. Chem. Soc.* **2018**, *140*, 12434.
[8] H. Oveisi, S. Rahighi, X. Jiang, Y. Nemoto, A. Beitollahi, S. Wakatsuki, Y. Yamauchi, *Chem. - Asian J.* **2010**, *5*, 1978.
[9] J. Wang, Y. Xu, B. Ding, Z. Chang, X. Zhang, Y. Yamauchi, K. C. W. Wu, *Angew. Chem., Int. Ed.* **2018**, *57*, 2894.
[10] S. Choudhury, D. Fischer, P. Formanek, M. Stamm, L. Ionov, *Adv. Mater. Interfaces* **2018**, *5*, 1701116.
[11] L. Yao, Q. Wu, P. Zhang, J. Zhang, D. Wang, Y. Li, X. Ren, H. Mi, L. Deng, Z. Zheng, *Adv. Mater.* **2018**, *30*, 1706054.
[12] Z. Yang, J. Wang, K. Huang, J. Ma, Z. Yang, Y. Lu, *Macromol. Rapid Commun.* **2008**, *29*, 442.
[13] D. Zhao, J. Feng, Q. Huo, N. Melosh, G. H. Fredrickson, B. F. Chmelka, G. D. Stucky, *Science* **1998**, *279*, 548.
[14] W. C. Chu, S. F. Chiang, J. G. Li, S. W. Kuo, *RSC Adv.* **2014**, *4*, 784.
[15] C. Liang, S. Dai, *J. Am. Chem. Soc.* **2006**, *128*, 5316.
[16] W. C. Chu, S. F. Chiang, J. G. Li, S. W. Kuo, *Materials* **2013**, *6*, 5077.
[17] B. P. Bastakoti, S. Ishihara, S. Y. Leo, K. Ariga, K. C. W. Wu, Y. Yamauci, *Langmuir* **2014**, *30*, 651.
[18] C. W. Wu, Y. Yamauchi, T. Ohsuna, K. Kuroda, *J. Mater. Chem.* **2006**, *16*, 3091.
[19] V. Malgras, J. Henzie, T. Takei, Y. Yamauchi, *Angew. Chem., Int. Ed.* **2018**, *57*, 8881.
[20] D. Hu, Z. Xu, K. Zeng, S. Zheng, *Macromolecules* **2010**, *43*, 2960.
[21] Y. Deng, T. Yu, Y. Wang, Y. Shi, Y. Meng, D. Gu, L. Zhang, Y. Huang, C. Liu, X. Wu, D. Zhao, *J. Am. Chem. Soc.* **2007**, *129*, 1690.
[22] Y. Deng, C. Liu, D. Gu, T. Yu, B. Tu, D. Zhao, *J. Mater. Chem.* **2008**, *18*, 91.
[23] S. W. Kuo, C. L. Lin, F. C. Chang, *Macromolecules* **2002**, *35*, 278.
[24] C. F. Huang, S. W. Kuo, F. J. Lin, W. J. Huang, C. F. Wang, W. Y. Chen, F. C. Chang, *Macromolecules* **2006**, *39*, 300.
[25] C. F. Huang, S. W. Kuo, H. C. Lin, J. K. Chen, Y. K. Chen, H. Xu, F. C. Chang, *Polymer* **2004**, *45*, 5913.
[26] J. G. Li, Y. D. Lin, S. W. Kuo, *Macromolecules* **2011**, *44*, 9295.
[27] J. G. Li, C. Y. Chung, S. W. Kuo, *J. Mater. Chem.* **2012**, *22*, 18583.
[28] J. G. Li, R. B. Lin, S. W. Kuo, *Macromol. Rapid Commun.* **2012**, *33*, 678.
[29] J. G. Li, W. C. Chu, U. Jeng, S. W. Kuo, *Macromol. Chem. Phys.* **2013**, *214*, 2115.
[30] W. C. Chu, L. Dai, J. K. Chen, C. F. Huang, S. W. Kuo, *J. Nanosci. Nanotechnol.* **2016**, *16*, 9805.
[31] W. C. Chu, C. Young, B. P. Bastakoti, Y. Yamauchi, S. W. Kuo, *Chem. - Eur. J.* **2017**, *23*, 13734.
[32] J. G. Li, Y. F. Ho, H. C. Liang, M. M. M. Ahmed, S. W. Kuo, *Chem. - Eur. J.* **2019**, *25*, 10456.
[33] S. W. Kuo, *Hydrogen Bonding in Polymeric Materials*, John Wiley & Sons, Hoboken, NJ **2018**.
[34] J. G. Li, W. C. Chu, C. W. Tu, S. W. Kuo, *J. Nanosci. Nanotechnol.* **2013**, *13*, 2495.
[35] O. Altukhov, S. W. Kuo, *RSC Adv.* **2015**, *5*, 22625.
[36] M. W. Huang, S. W. Kuo, H. D. Wu, F. C. Chang, S. Y. Fang, *Polymer* **2002**, *43*, 2479.
[37] S. W. Kuo, F. C. Chang, *Macromol. Chem. Phys.* **2002**, *203*, 868.
[38] A. F. El-Mahdy, Y. H. Hung, T. H. Mansoure, H. H. Yu, T. Chen, S. W. Kuo, *Chem. - Asian J.* **2019**, *14*, 1429.
[39] A. F. M. EL-Mahdy, C. Young, J. Kim, J. You, Y. Yamauchi, S. W. Kuo, *ACS Appl. Mater. Interfaces* **2019**, *11*, 9343.
[40] H. Zhang, M. Lu, H. Wang, Y. Lyu, D. Li, S. Sun, J. Shi, W. Liu, *Sustainable Energy Fuels* **2018**, *2*, 2314.
[41] L. Yu, L. Hu, B. Anasori, Y.-T. Liu, Q. Zhu, P. Zhang, Y. Gogotsi, B. Xu, *ACS Energy Lett.* **2018**, *3*, 1597.
[42] R. Heimböckel, S. Kraas, F. Hoffmann, M. Froba, *Appl. Surf. Sci.* **2018**, *427*, 1055.
[43] H. R. Abuzeid, A. F. M. El-Mahdy, M. M. M. Ahmed, S. W. Kuo, *Polym. Chem.* **2019**, *10*, 6010.
[44] A. F. M. EL-Mahdy, C. H. Kuo, A. Alshehri, C. Young, Y. Yamauchi, J. Kim, S. W. Kuo, *J. Mater. Chem. A* **2018**, *6*, 19532.
[45] A. Halder, M. Ghosh, A. K. M , S. Bera, M. Addicoat, H. S. Sasmal, S. Karak, S. Kurungot, R. Banerjee, *J. Am. Chem. Soc.* **2018**, *140*, 10941.
[46] M. M. M. Ahmed, T. Imae, J. P. Hill, Y. Yamauchi, K. Ariga, L. K. Shrestha, *Colloids Surf., A* **2018**, *538*, 127.
[47] R. Pujari, A. Lokhande, A. Shelke,J. Kim, C. Lokhande, *J. Colloid Interface Sci.* **2017**, *496*, 1.
[48] W. C. Chen, M. M. M. Ahmed, C.-F. Wang, C.-F. Huang, S. W. Kuo, *Polymer* **2019**, *185*, 121940.
[49] D. Saha, Y. Li, Z. Bi, J. Chen, J. K. Keum, D. K. Hensley, H. A. Grappe, H. M. Meyer, S. Dai, M. P. Paranthaman, A. K. Naskar, *Langmuir* **2014**, *30*, 900.
[50] M. G. Mohamed, A. F. M. El-Mahdy, M. M. M. Ahmed, S. W. Kuo, *ChemPlusChem* **2019**, *84*, 1767.
[51] J. L. Goldfarb, G. Dou, M. Salari, M. W. Grinstaff, *ACS Sustainable Chem. Eng.* **2017**, *5*, 3046.

